Inorg. Chem. **2004**, *43*, 436–442

$R_6TT'_2$, New Variants of the Fe_2P Structure Type. Sc_6TTe_2 (T = Ru, Os, Rh, Ir), Lu_6MoSb_2, and the Anti-typic $Sc_6Te_{0.80}Bi_{1.68}$

Ling Chen and John D. Corbett*

Department of Chemistry, Iowa State University, Ames, Iowa 50011

Received August 13, 2003

The Fe_2P structure ($P\bar{6}2m$) features two 3-fold Fe positions and both 2-fold and 1-fold P sites, and variations in occupancies of the latter pair yield the reported diversity of results. The known Sc_6TTe_2 examples for T = Fe–Ni are herein extended to four heavier transition metal T derivatives. An attempt to synthesize bismuth analogues led to the novel inverse derivative in which fractional Te (vice T) occupies the smaller tricapped trigonal prismatic (TTP) Sc polyhedron, and Bi rather than Te occurs in the larger TTP of Sc, with parallel reversal of polarity in the bonding. The reported Lu_8Te, which is distributed as Lu_6TeLu_2, is the only example in which a transition metal occupies the normal 2-fold P or Te non-metal position, with corresponding large effects on the bonding. Lutetium otherwise does not form R_6TTe_2 analogues, but the novel Lu_6MoSb_2 isotype occurs instead. Extended Hückel calculations are presented for five examples, and the structural and bonding regularities and varieties are discussed further.

Introduction

Metal-rich compounds formed between an early transition metal, a late transition metal, and a late main-group element (non-metal) exhibit a variety of novel stoichiometries, structures, and bonding. All of these appear to reflect the unusually strong bonding that occurs between early and late transition metals, as first noted by Brewer in intermetallic systems.[1] A large group of such ternary phases occur as metal-rich halides, both as isolated clusters and in extended chain motifs.[2,3] Chalcogen and pnictogen compounds with early−late transition metal combinations yield a completely different group of compounds that are generally more metal-rich and, accordingly, more two- or three-dimensional in metal−metal bonding. The largest group has been reported among ternary compounds of the rare-earth elements, scandium in particular, with tellurium. These include the families of orthorhombic $Sc_5Ni_2Te_2$,[4] orthorhombic $Y_5T_2Te_2$, T = Fe, Co, Ni[5] (with metal columns rather than sheets), orthorhombic Sc_6TTe_2, T = Pd,[5] Ag, Cu, Cd,[6] the tetragonal chain phase $Sc_{14}T_3Te_8$, T = Ru, Os,[7] and two groups with the hexagonal Fe_2P-type structures, Sc_6TTe_2, T = Fe − Ni,[8] and Dy_6TTe_2, T = Fe−Ni.[9] To these can be added the zirconium analogues Zr_6TTe_2, T = Mn − Ni, Ru, Pt[10] and $Hf_6Ni_{1-x}Sb_{2+x}$, $x \sim 0.25$.[11]

The well-known hexagonal Fe_2P-type structure[12,13] is exhibited by hundreds of alloys and intermetallic compounds. One distinctive feature of this structure type is that both the iron and phosphorus sites are double, viz., Fe(I), Wyckoff site 3f, Fe(II) 3g, P(I) 1b, and P(II) 2c or, literally, as Fe_6P_3. Thus, many mixed but ordered compositions are possible in higher order compounds. Mixed metals on the two Fe sites appear more common, and phases such as ZrNbP[14,15] and RAgGe, R = Y, Sm, Gd−Lu,[16] occur as ordered intermetallics.[17]

Compounds in which the two phosphorus sites are distinguished by different elements are principally an inter-

* Author to whom correspondence should be addressed. E-mail: jdc@ameslab.gov.

(1) Brewer, L.; Wengert, P. R. *Metall. Trans.* **1973**, *4*, 83.
(2) Corbett, J. D. *J. Alloys Compd.* **1995**, *229*, 10.
(3) Corbett, J. D. *Inorg. Chem.* **2000**, *39*, 5178.
(4) Maggard, P. A.; Corbett, J. D. *Inorg. Chem.* **1999**, *38*, 1945.
(5) Maggard, P. A.; Corbett, J. D. *J. Am. Chem. Soc.* **2000**, *122*, 10740.
(6) Chen, L.; Corbett, J. D. *Inorg. Chem.* **2002**, *41*, 2146.
(7) Chen, L.; Corbett, J. D. *J. Am. Chem. Soc.* **2003**, *125*, 1170.
(8) Maggard, P. A.; Corbett, J. D. *Inorg. Chem.* **2000**, *39*, 4143.
(9) Bestaoui, N.; Herle, S.; Corbett, J. D. *J. Solid State Chem.* **2000**, *155*, 9.
(10) Wang, C.; Hughbanks, T. *Inorg. Chem.* **1996**, *35*, 6987.
(11) Kleinke, H. *J. Alloys Compd.* **1998**, *270*, 136.
(12) Hyde, B. G.; Andersson, S. *Inorganic Crystal Structures*; J. Wiley: New York, 1989; p 88.
(13) Rundqvist, S.; Jellinek, F. *Acta Chem. Scand.* **1959**, *13*, 425.
(14) Miller, G.; Cheng, J. *Inorg. Chem.* **1995**, *34*, 2962.
(15) Marking, G.; Franzen, H. F. *J. Alloys Compd.* **1994**, *204*, L16.
(16) Gibson, G.; Pöttgen, R.; Kremer, R. K.; Simon, A.; Ziebeck, K. R. A. *J. Alloys Compd.* **1996**, *239*, 34.
(17) Dwight, A. E. *J. Less-Common Met.* **1973**, *30*, 1.

10.1021/ic0302581 CCC: $27.50
Published on Web 12/23/2003

Table 1. Some Reaction Compositions, Conditions, and Products

loading	reactions[a]	source; product phase analysis[b]
Sc_6RuTe_2	arc melt; HTF, 1135, 1 w	HTF; >95% Sc_6RuTe2 (Fe_2P)
Sc_6OsTe_2	arc melt; HTF, 1300, 1 w	HTF; 85% Sc_6OsTe (Fe_2P),[c] 15% ScTe (NiAs)
Sc_6RhTe_2	arc melt;	90% Sc_6RhTe_2 (Fe_2P),[c] 10% ScTe (NiAs)
	HTF, 1300, 48 h	85% Sc_6RhTe_2 (Fe_2P), 15% ScTe (NiAs)
Sc_6IrTe_2	arc melt;	>95% Sc_6IrTe_2 (Fe_2P)
	HTF, 1300, 48 h	>90% Sc_6IrTe_2 (Fe_2P), ~10% ScTe (NiAs)
Sc_6PtTe_2	arc melt	90% Sc_6PtTe_2 (Sc_6PdTe_2 type[d]), 10% ScTe (NiAs)
	HTF, 1300, 48 h	85% Sc_6PtTe_2, 15% ScTe (NiAs)
Sc_6PdTe_2	tube furn., 1050, 72 h	95% Sc_6PdTe_2 (Sc_6PdTe_2 type[d])
Lu_7Sb	arc melt; HTF, 1200, −	90% Lu_6MoSb_2[e] (Fe_2P type)[c]

[a] HTF = high-temperature vacuum furnace, °C. [b] All products identified by Guinier X-ray powder diffraction. [c] Data crystal for X-ray diffraction solution as well. [d] Reference 5. [e] See text.

metallic example, such as Zr_6CoAl_2[18] and the $R_6TT'_2$ types noted above in which R may be Sc, Y, or Dy, T is a late transition metal, and T′ is Te or, in one case, Sb, although examples with other R or other main-group elements are presumably feasible. Here, we report some additional diverse compounds of the Fe_2P-type family that nicely demonstrate more of the structural and electronic flexibility of the parent type: (1) Sc_6TTe_2 with T being the 4d or 5d elements Ru, Os, Rh, and Ir as derivatives of Sc_6FeTe_2,[8] (2) Lu_6MoSb_2 as the first example of a lutetium antimonide under the circumstance that Lu_6TTe_2 analogues do not appear to be stable, and (3) the anti-type example $Sc_6Te_xBi_{2x}$ ($x \sim 0.8$) in which only main-group elements occupy both phosphorus sites and with a reversal of the usual disposition according to electronegativity. Another anti-example occurs in the newly discovered Lu_8Te.[19] This has a parallel distribution as Lu_6TeLu_2, but the bonding has not been considered before in any detail.

Experimental Section

Syntheses. All reactions were loaded in a glovebox filled with Ar. The rare-earth metals Sc (chunk) and Lu (powder) were used as supplied from Ames Laboratory (99.99%), the late transition metals Ru, Os, Rh, and Ir as powders from Alfa (>99.5%), and Te ingots, Bi pieces and Sb powder were from Aldrich (99.99%). The purities of all starting elements were checked by EDS analyses as well.

All compounds were synthesized by typical solid-state chemistry methods on a scale of about 300 mg total. Some details are listed in Table 1. For each reaction, a pressed $^1/_4$ in. diameter pellet of the appropriate mixture was first arc-melted for 20 s with ~40 amp current on a water-cooled copper hearth in the Ar atmosphere within a glovebox after Zr shot had first been melted to purify further the atmosphere. (The minimum current was utilized for the Bi reaction.) The sample pellet was subsequently inverted and arc-melted again to promote homogenization. The total weight losses after arc-melting because of volatilization were under 4% unless noted. The buttons were crushed into smaller pieces in an agate mortar and then ground into a fine black powder for Guinier X-ray powder examinations so as to identify crystalline phases at that point. The powders were then pelletized again, wrapped in molybdenum foil, and sealed into tantalum tubing. The molybdenum foil helped to protect (at least) the inner wall of the Ta container from direct reaction with the late transition metal components (and with Te in the Bi reaction) at high temperatures. (Some may still erode the Ta tubing as well as the Mo foil itself, but to a much smaller extent.) Some slow decomposition with time at 1300 °C is evident in many systems (Table 1).

The best way to synthesize pure Sc_6MTe_2 phases is via annealing at 1000 °C for 1 week without arc-melting and with the Ta held within sealed evacuated silica jackets and heated in conventional tube furnaces. The best way to grow diffraction-size single crystals is via annealing the arc-melted products at 1300 °C for 48 h followed by slow cooling to room temperature. The latter was done in a graphite-heated vacuum furnace (if >1100 °C) with a residual pressure less than 10^{-6} Torr. which also eliminates any possibility of hydrogen impurities. Usually, the samples partially melted in the early stages, and small crystals that were suitable for single-crystal X-ray diffraction could be picked from the product or from the inner Mo surface. The yields of the target compounds according to relative intensities of the Guinier powder diffraction components were generally pretty high (>85%). All the reactions with Ru, Os, Rh, and Ir succeeded on the first try. All the compounds are stable in air at room temperature for a couple of months, and crystals of $Sc_6Te_{0.8}Bi_{1.6}$ are so stable for more than a year. Similar reactions were also established in the Sc−Pd−Te and Sc−Pt−Te systems, but these form the orthorhombic Sc_6TTe_2 (Sc_6PdTe_2 type, derived from Sc_2Te[6]) instead, as do Y_6TTe_2 (T = Pd, Pt).[20] The last is interesting in that the parent binary member Y_2Te cannot be synthesized, in contrast to Sc_2Te.[21]

A wide variety of similar reactions in the Sc−Bi−Te system all failed to give any comparable Sc_6BiTe_2-type phase, producing instead orthorhombic Sc_5Bi_3[22] cubes, ScTe (NaCl) sheets, and leftover Sc. Nonetheless, a few rod crystals that gave the structure of, and analyzed as, the anti-type $Sc_6Te_{0.80}Bi_{1.68}$ (below) were picked from the surface of the Mo foil after reaction of the arc-melted button at 1300 °C for 48 h. This and the Ta inner wall were also covered with well dispersed smaller crystals, probably Sc_5Bi_3. Variations in reaction temperature or prior treatment were not as useful. The physical separation of the leftover Sc from the initial reaction (2.5 mol of Sc/mol of Sc_5Bi_3 for a loaded Sc_6TeBi_2 composition) appeared to be a major limitation. We assume that the well-isolated rods of $Sc_6Te_{0.8}Bi_{1.6}$ grew instead by a customarily not-very-efficient, dynamic vapor phase transport reaction, doubtlessly autogenous in nature, as with ZrCl.[2] Compositions determined by single-crystal structural refinements of two crystals were $Sc_6Te_{0.79(1)}Bi_{1.63(1)}$ and $Sc_6Te_{0.797(5)}Bi_{1.682(8)}$ which are in accord with the EDS results for the latter, in at. %. Calcd [found]: Sc, 70.8

(18) Krypyakevich, P. I.; Burnashova, V. V.; Markiv, V. Ya. *Depov. Akad. Nauk. Ukr. RSR, Ser. A.: Fiz-Tekhn. Met. Nauk.* **1970**, *32*, 828.
(19) Chen, L.; Corbett, J. D. *J. Am. Chem. Soc.* **2003**, *125*, 7794.
(20) Chen, L.; Corbett, J. D. Unpublished research.
(21) Maggard, P. A.; Corbett, J. D. *Angew. Chem., Int. Ed. Engl.* **1997**, *36*, 1974.
(22) Haase, M.; Block, H.; Jeitschko, *W. Z. Anorg. Allg. Chem.* **2001**, *627*, 1941.

Table 2. Lattice Dimensions of $R_6TT'_2$ (Fe_2P-Type) Phases, R = Sc, Lu; T = Ru, Os, Rh, Ir, Te, Mo; T′ = Te, Sb, Bi, Lu

compounds	*a* (Å)	*b* (Å)	*V* (Å^3)
Sc_6RuTe_2[a]	7.681(1)	3.844(2)	196.4(1)
Sc_6OsTe_2[b]	7.627(2)	3.864(1)	194.67(9)
Sc_6RhTe_2[b]	7.718(1)	3.8379(7)	197.98(5)
Sc_6IrTe_2[a]	7.681(8)	3.853(4)	196.8(4)
$Sc_6Te_{0.797(5)}Bi_{1.680(8)}$[b]	7.6821(3)	4.0815(4)	208.60(2)
Lu_6TeLu_2[b,c]	9.000(3)	3.687(2)	258.6(2)
Lu_6MoSb_2[b]	7.935(1)	4.2630(9)	232.43(7)

[a] Lattice parameters determined from Guinier powder data, ≥12 lines indexed. [b] Lattice parameters and composition determined from single-crystal data. [c] Reference 19.

[74.0(6)]; Te, 9.40 [9.3(8)]; Bi, 19.8 [16.7(8)]. This was equivalent to $Sc_{6.00(5)}Te_{0.75(7)}Bi_{1.35(7)}$. The latter examination should eliminate all significantly stabilizing impurity elements heavier than B, whereas the high vacuum precludes a hydride. Otherwise, we do not understand the substoichiometry.

Following the surprising discovery of Lu_8Te,[19] natural curiosity led us to load parallel Lu−Sb reactions. The compositions Lu_7Sb and Lu_9Sb_2 both gave a major Fe_2P-type product by powder diffraction analysis, tentatively Lu_2Sb, but single crystal structural refinements of crystals from both reactions gave only about 75% Sb occupancy of the 1b site. But a test for phase breadth via four more reactions loaded between 31 and 38 at. % Sb instead all gave as the main products Lu_7Sb_3[20] (Sc_7As_3 type[23]) plus LuSb (NaCl) in the powder patterns. An EDS check helped us to clarify that the apparent Sb-deficient occupancy of the 1c site from single-crystal results were instead those for Lu_6MoSb_2 [at. % calcd [found]: Lu, 66.7 [62(4)]; Mo, 11.1 [11.1(6)]; Sb, 22.2 [27(2)]], or $Sc_{6.0(4)}Mo_{1.07(6)}Sb_{2.6(2)}$. The two reactions that gave this phase also produced distinctly brittle Mo foil, the Mo source. Other T explorations yielded a series of new orthorhombic $Lu_7T_2Te_2$ phases.[24]

X-ray Crystallography. All single-crystal data sets were collected at room temperature with the aid of a Bruker AXS SMART APEX CCD-based X-ray diffractometer and monochromatized Mo Kα radiation. Lattice constants are given in Table 2, and some crystallographic details are listed in Table 3. Given the clear powder pattern identifications, most structures were solved[25,26] assuming the Fe_2P-type space group $P\bar{6}2m$. In accord, the mean values of $|E^2 - 1|$ in all cases strongly suggested that the structures were noncentrosymmetric. Table 4 lists the positional and displacement parameters and site occupancies (≠1) for the four representative compounds in the standard setting.[13] Both Sc_6OsTe_2 and $Sc_6Te_{0.797(5)}Bi_{1.682(8)}$ crystals were racemic twins, the components twinning under the law [−1 0 0, 0 −1 0, 0 0 −1] with minor components of 18.01% and 18.48%, respectively. For Sc_6RhTe_2, although Rh at the 1b site has a large isotropic parameter compared with that for Te, this is not the Fe_2P-type binary compound "Sc_6Te_3" according to the high synthetic yield. The occupancy of Rh freely refined to 100.7(7)% with this thermal parameter; in addition, a binary compound with this structure is not known. The same thing happens with Sc_6OsTe_2, a larger 1b site thermal parameter but with full occupancy. In the case of $Sc_6Te_xBi_{2x}$, two crystals from the synthesis (above) both gave essentially the same results: $Sc_6Te_{0.79(1)}Bi_{1.63(1)}$ and $Sc_6Te_{0.797(5)}Bi_{1.682(8)}$. Also, the Bi:Te ratio was strongly supported by EDS results (above) from one of the single crystals. For Lu_6MoSb_2, once the presence of Mo was clarified by EDS, the structure was refined without event.

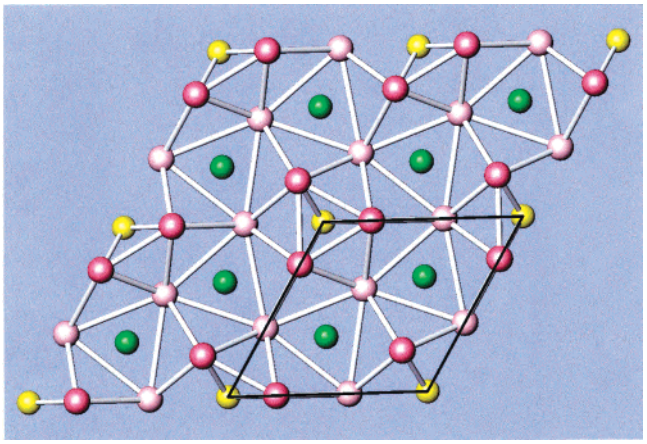

Figure 1. [001] section of the hexagonal $R_6TT'_2$ structure with the cell marked. Key: red, (3f) Sc or Lu; pink, (3g) Sc or Lu; yellow, (1b) Ru, Rh, Os, Ir, Mo or Te; green, (2c) Te, Bi, or Sb. All of the metal−metal contacts are marked up through 5.0 Å.

Results and Discussion

Crystal Structure. The overall structure of most ternary $R_6TT'_2$ (Fe_2P-based) compounds projected along [001] is shown in Figure 1, with a bond cutoff in the drawing of 5.0 Å. All atoms lie on mirror planes, the 3f and 2c (red, green) atoms at $z = 0$, and the 3g and 1b (pink, yellow) atoms at $z = 1/2$. In the parent structure, 3f and 3g are occupied by Fe, and the independent 2c and 1b both contain P, but in an appreciable range of ternary members, the 3f and 3g (red, pink) sites are usually occupied by the same early metal, the 1b site (yellow) is usually favored for a later transition metal, and, up to recent times, 2c (green) always belonged to a main group element. This gives the families R_6TTe_2 (R = Sc,[8] Dy;[9] T = Fe, Co, Ni), Zr_6TTe_2 (T = Mn−Ni, Ru, Pt),[10] Zr_6CoAl_2,[18] Zr_6FeSn_2,[27] and Hf_6TSb_2 (T = Fe,Co,Ni).[11] To these are here added Sc_6TTe_2, T = Ru, Rh, Os, and Ir, and Lu_6MoSb_2.

The general motif of this $R_6TT'_2$ structure type—Figure 1—consists of centered tricapped trigonal prisms (TTP) further condensed to form the 3-D hexagonal structure. There are two kinds of confacial TTPs: the smaller metal one (red) centered by a (yellow) (T) atom and two larger metal ones (pink) centered by the green (T′) element. Both share their triangular faces with like polyhedra to generate chains along [001]. Each rectangular face of the trigonal prisms is outer-capped by the other R element type. Finally, the 2c-centered TTP are interconnected with 1b-centered TTPs through relatively short (strong) inner−outer R−R interactions. Usually, the 1b site (yellow) surrounded by the smaller trigonal prism is occupied by a relatively smaller, late transition metal (T = Mn, Fe − Ni, Ru, Rh, Os, Ir). Data on the six new compounds reported here are given in Tables 1 and 2 and, for the four structures refined, in Tables 3 and 4. Table 5 summarizes specific and average bond distances of different types in the latter four $R_6TT'_2$ compounds.

The antitype $Sc_6Te_{0.8}Bi_{1.6}$ shows a very nice site preference, which may simply arise because Bi is larger than Te

(23) Berger, R.; Nolaeng, B. I.; Tergenius, L. E. *Acta Chem. Scand.* **1981**, *A35*, 679.
(24) Chen, L.; Corbett, J. D. *Inorg. Chem.*, accepted.
(25) SHELXTL6.10. Bruker AXS, Inc.: Madison, WI, 2000.
(26) Blessing, R. H. *Acta Crystallogr.* **1995**, *A51*, 33.
(27) Kwon, Y.-U.; Sevov, S. C.; Corbett, J. D. *Chem. Mater.* **1990**, *2*, 550.

Table 3. Some Data Collection and Refinement Parameters[a]

empirical formula	Sc_6RhTe_2	Sc_6OsTe_2	$Sc_6Te_{0.797(5)}Bi_{1.682(8)}$	Lu_6MoSb_2
fw	627.87	715.16	722.9	1389.26
space group, Z	$P\bar{6}2m$ (No. 189),1	$P\bar{6}2m$ (No. 189),1	$P\bar{6}2m$ (No. 189),1	$P\bar{6}2m$ (No. 189),1
abs. coeff, mm^1	13.976	28.397	49.914	69.973
d_{calc}, Mg/m^3	5.266	6.100	5.76	9.925
R1, wR2 [$I > 2\sigma_I$]	0.0139, 0.0333	0.0166, 0.0489	0.0105, 0.0240	0.0176,0.0391
R1, wR2 (all data)[b]	0.0139, 0.0333	0.0167, 0.0490	0.0105, 0.0240	0.0176, 0.0391

[a] Lattice parameters in Table 2. [b] In the majority of cases, all allowed reflections were also observed ($>2\sigma_I$).

Table 4. Positional and Equivalent Isotropic Displacement Parameters ($\times 10^3$) for Four $Sc_6TT'_2$ Structures

atom	Wyckoff site	x	y	z	U(eq)	site occ. ($\neq 1$)
		Sc_6RhTe_2				
Sc1	3f	0.2420(2)	0	0	14(1)	
Sc2	3g	0.6068(2)	0	1/2	16(1)	
Te	2c	1/3	2/3	0	12(1)	
Rh	1b	0	0	1/2	24(1)	
		Sc_6OsTe_2[a]				
Sc1	3f	0.2386(3)	0	0	7(1)	
Sc2	3g	0.6126(4)	0	1/2	8(1)	
Te	2c	1/3	2/3	0	5(1)	
Os	1b	0	0	1/2	16(1)	
		$Sc_6Te_{0.797(5)}Bi_{1.682(8)}$[a]				
Sc1	3f	0.2373(2)	0	0	10(1)	
Sc2	3g	0.6076(2)	0	1/2	9(1)	
Bi	2c	1/3	2/3	0	10(1)	0.841(4)
Te	1b	0	0	1/2	10(1)	0.797(5)
		Lu_6MoSb_2[a]				
Lu1	3f	0.2407(1)	0	0	7(1)	
Lu2	3g	0.6041(1)	0	1/2	8(1)	
Sb	2c	1/3	2/3	0	8(1)	
Mo	1b	0	0	1/2	9(1)	

[a] Refined component has been converted to standard setting.

(1.51 vs 1.37 Å in metallic radii[28]) and then naturally fits the larger TTP better. (Note that both main-group element sites are only about 80% occupied.) From Os to Bi, the trigonal faces of two TTP do not change much (Table 5), but they are 0.22 Å farther apart along the *c* direction with Bi owing to differences in something akin to the van der Waals radii. This size-determined site preference is evidently again the case with Lu_8Te,[19] the first example with the principal metallic element also occupying the nominally interstitial 2c site. In the case of Lu_6MoSb_2, the Lu1−Lu1 interaction is the shortest among all Lu−Lu distances, in parallel with the strong Lu−Mo interactions in the Mo-centered TTP of Lu1 at essentially the sum of single bond metallic radii.[28] These unusual site occupancies are well reflected in bonding differences as well (see below).

Figure 2 schematically summarizes the relationships among all of these Fe_2P-type intermetallics relative to the parent Sc_6FeTe_2. The subgroup $Sc_6(Ru/Os)Te_2$ phases are isoelectronic compounds, and these T elements can also be substituted by Co, Rh, or Ir, their respective neighbors in the periodic table. Some of the same substitutions are found with the Dy_6TTe_2 subgroup.[9] Interestingly, the slightly electron-richer Pt and Pd examples of Sc_6TTe_2 do not crystallize in the Fe_2P structure, but in an orthorhombic sheet structure related to that of Sc_2Te.[6,21] We report here the first evidence that the types of atoms at 2c and 1b sites in the

(28) Pauling, L. *Nature of the Chemical Bond*, 3rd ed.; Cornell University Press: Ithaca, NY, 1960; p 403.

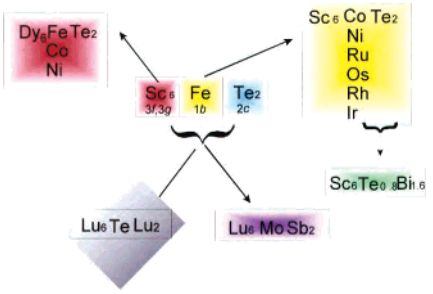

Figure 2. Groups of diverse intermetallic compounds with an Fe_2P structure type that are discussed in the present paper. The arrows indicate how the compounds are derived from the Sc_6FeTe_2 parent through chemical substitution. 3f, 3g, 1b, and 2c are Wyckoff symbols for the four independent crystallographic sites.

crystal structure can also be interchanged, e.g., with Te and Bi, to yield the evidently novel antitype $Sc_6Te_{0.8}Bi_{1.6}$. Substitution of Sc by Lu (or Dy) is not a surprise, but the fact that Lu atoms themselves can also occupy the 2c site in Lu_6TeLu_2 is, illustrating not only a presumed size effect but also the electronic flexibility of this type of structure. Again, the discovery of the electron poorer Lu_6MoSb_2, the first lutetium antimonide, also shows that Te and Sb have similar chemical properties in this metal-rich intermetallic system.

As described before,[8] the Sc_6TTe_2 (M = Fe, Co, Ni) compounds exhibit a dominant one-dimensionality of metal−metal bonding within the TTP chain along the *c* direction in terms of bond distance as well as Mulliken overlap populations (MOP). In contrast, Zr_6TTe_2 (T = Mn−Ni, Ru, Pt) phases[10] with electron-richer transition metals have metal−metal bonding arrays that have been described as fully three-dimensional, corresponding to greater filling of the broad conduction band. However, the opposite trend is seen on comparing the electron-poor Lu_8Te (Lu_6TeLu_2, VEC = 30) with Sc_6OsTe_2 (VEC = 38), in which the metal−metal array in the former is more three-dimensional because of the greater delocalization achieved with the metallic lutetium in the 2c sites provides stronger metal−metal bonding. (This aspect is considered in the next section.)

Theoretical Calculations and Comparisons. To gain further understanding of the characteristics and differences among these compounds, extended Hückel calculations were carried out within the tight-binding approximation for the Sc_6RuTe_2, Sc_6OsTe_2, "Sc_6TeBi_2", Lu_6MoSb_2, and Lu_8Te examples with the aid of the CAESAR program.[29] To make the results more appropriate to the charge distributions in these unconventional compounds and also more comparable to each other, interated H_{ii} parameters of Sc and Te were taken from Sc_6FeTe_2,[8] whereas such data for Fe, Ru, Os,

Table 5. Selected and Average Bond Distances (Å) in Some $R_6TT'_2$ Compounds

atom pairs	Sc_6RhTe_2	Sc_6OsTe_2	$Sc_6Te_{0.80(1)}Bi_{1.68(1)}$	Lu_6MoSb_2	Lu_8Te[a]
R1−R1	3.235(3)	3.152(4)	3.158(2)	3.308(1)	4.318(2)
R2−R2	4.114(3)	4.095(4)	4.096(2)	4.217(1)	4.835(3)
R1−R2, av	3.32	3.30	3.39	3.51	3.59
i−o, small TTP	3.273(1) (×4)	3.223(2) (×4)	3.3287(8) (×4)	3.4728(6) (×4)	3.611(2) (×4)
o−i, large TTP	3.407(2) (×2)	3.448(3) (×2)	3.501(2) (×2)	3.5856(8) (×2)	3.545(2) (×2)
R1−T (3f−1b)	2.678(1)	2.654(2)	2.7365(8)	2.8619(6)	3.100(2)
R1−T′ (3f−2c)	2.988(1)	2.970(2)	2.9983(8)	3.0790(6)	3.283(2)
R2−T (3g−1b)	3.035(2)	2.951(3)	3.015(1)	3.1416(8)	3.479(2)
R2−T′ (3g−2c)	3.0537(6)	3.054(1)	3.1250(4)	3.2360(4)	3.345(1)

[a] Lu_6TeLu_2, ref 19.

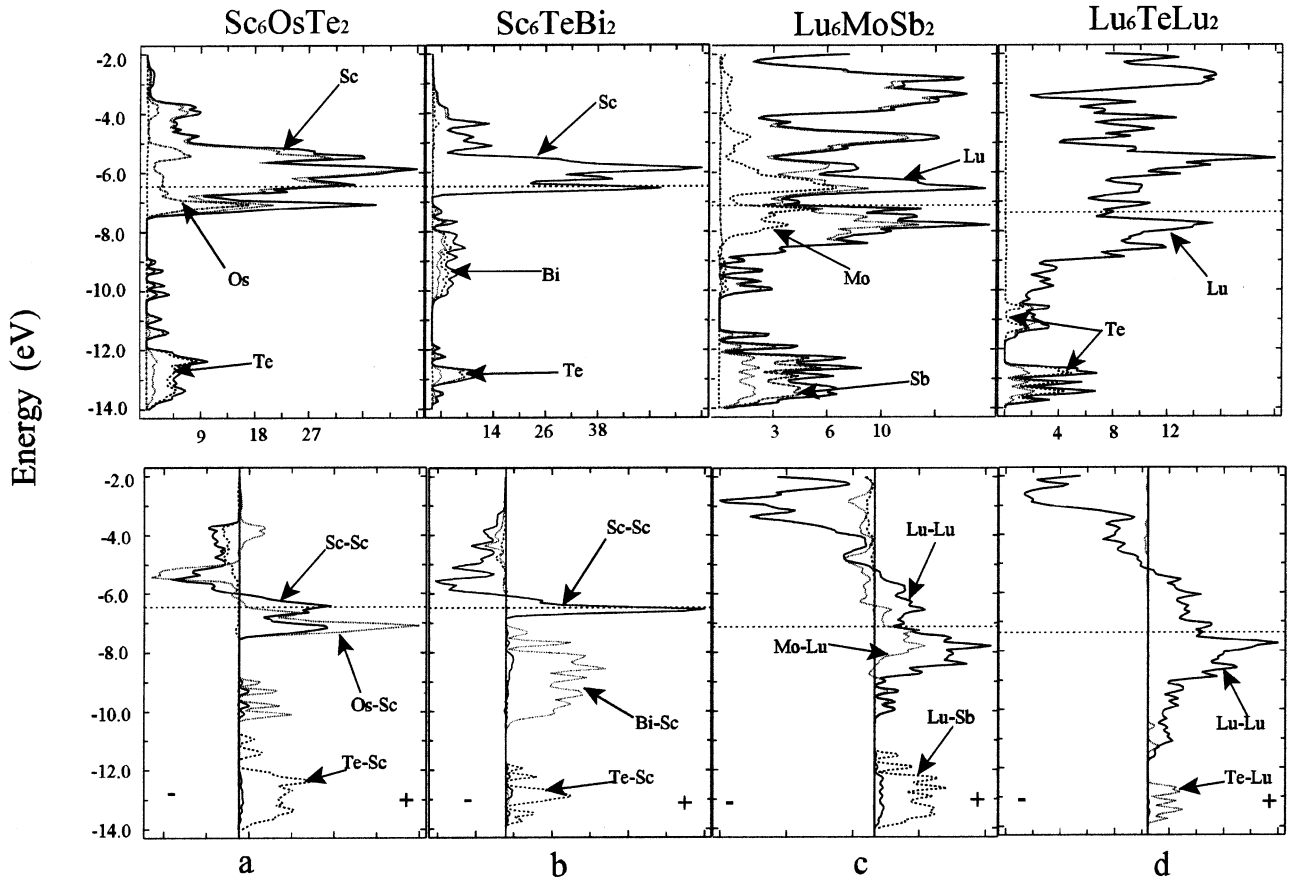

Figure 3. DOS (upper) and COOP (lower) data for $R_6TT'_2$ compounds: (a) Sc_6OsTe_2; (b) Sc_6TeBi_2; (c) Lu_6MoSb_2; (d) Lu_8Te (Lu_6TeLu_2). The horizontal dashed lines mark the Fermi levels.

and Lu were obtained from a full charge-iterative calculations in which orbital energy parameters for these atoms were varied to self-consistency as a function of Mulliken charge transfer. The Sb and Bi parameters and the standard orbital exponents were taken from Alvarez,[30] and Mo parameters were estimated from those of Zr[10] and Ru. All parameters used are listed in Supporting Information in Table S3.

Figure 3 shows the total and some partial densities-of-states (DOS) (top) and COOP (crystal orbital overlap population) (bottom) plots for four of the $R_6TT'_2$ phases in the energy range of −14.0 to −2.0 eV. For Sc_6OsTe_2 (a), the states from −14.0 to −10.5 eV correspond to Te(p)−Sc interactions. The four small peaks around −10.5 to −8.5 eV represent mainly Os(s)−Sc1p bonding states, whereas the pronounced peak at −7.0 eV originates mainly from Os d and Sc1 d states, with smaller contributions from Sc2 = d. The states above E_F are mainly Sc d states with some Os d and are initially bonding, as is usual in these electron-poor phases. There is a clear distinction between nearest-neighbor Sc1−Os intermetallic bonding interactions, which fall just below (and above) E_F, and the more polar Sc2−Te bonding which falls lower (−12 to −14 eV) with a counter antibonding states above E_F. (This effect is familiar in many metal-rich Sc−Te phases, in which it is reflected in lower Sc−Sc MOP values for those Sc with Te neighbors.[5,8]) This distinction is clear in the charges deduced for 3d Sc_6TTe_2 phases with T = Fe, Ru, and Os according to the Mulliken approximation, Table 6, namely Sc1 (−0.7 to −0.6 eV) vs

(29) Ren, J.; Liang, W.; Whangbo, M.-H. *CAESAR for Windows*; Prime-Color Software, Inc., North Carolina State University: Raleigh, NC, 1995.
(30) Alvarez, A. *Tables of Parameters for Extended Hückel Calculations, Parts 1 and 2*; Barcelona, Spain, 1987.

Table 6. Effective Atom Charges in Some $R_6TT'_2$ Phases as Calculated by Extended Hückel Means

	Sc_6FeTe_2[a]		Sc_6RuTe_2		Sc_6OsTe_2	
Wyckoff site	atom	charge	atom	charge	atom	charge
3f	Sc1	−0.71	Sc1	−0.70	Sc1	−0.58
3g	Sc2	0.47	Sc2	0.48	Sc2	0.69
2c	Te	−0.62	Te	−0.61	Te	−0.60
1b	Fe	1.98	Ru	1.92	Os	0.86
	Sc_6TeBi_2[b]		Lu_6TeLu_2		Lu_6MoSb_2	
Wyckoff site	atom	charge	atom	charge	atom	charge
3f	Sc1	−0.08	Lu1	0.29	Lu1	−0.41
3g	Sc2	0.05	Lu2	−0.01	Lu2	0.29
2c	Bi	0.21	Lu3	−0.32	Sb	−0.89
1b	Te	−0.36	Te	−0.2	Mo	2.14

[a] Reference 8. [b] Calculated with full occupancies.

Sc2 (+0.5 to +0.7 eV). Naturally, the most electronegative element Te has a negative charge, whereas the electron-rich T = Fe, Ru, and Os have positive effective charges, +2.0 dropping to +0.9 eV as the mixing with Sc becomes notably larger and the interactions become less polar with heavier period d elements. (Interestingly, these Sc1−T charge transfers are in the direction first postulated by Brewer and Wengert[1] from an acid−base viewpoint.)

The novel anti-typic $Sc_6Te_{0.8}Bi_{1.6}$ (calculated for full rather than ∼80% occupancies) exhibits a broader and less polar Bi(6p)−Sc2-based band at midenergies, whereas Te in the Sc1 TTP is now the more polar. Both effects level the approximate charges with only Te being somewhat negative and with Bi as a modest electron donor. E_F is barely lowered with the observed occupancies, $\sim Sc_6Te_{0.80}Bi_{1.68}$ (in a rigid band approximation), and only some nonbonding Sc−Te, Sc−Bi states are emptied. The conversion to Lu_6MoSb_2 shows two notable effects. First, the Lu−Lu interactions are strong and give rise to broader Lu−Lu bonding states, paralleling the similar behavior already discussed for Dy_2Te vs Sc_2Te[31] and broadening the empty portion of Lu−Lu bonding states (COOP) to −2 eV. The Lu−Sb(p) band and COOP are with better mixing lower and broader than, e.g., for Sc−Te, and the Lu−Mo band is broader, again giving appreciable charges to Sb and Mo, −0.9 and +2.1, respectively.

Finally Lu_8Te or, better for comparison, Lu_6TeLu_2 shows the largest changes (Figure 3d). The much broader conduction band and Lu−Lu COOP curves are striking, as the Lu−Lu states here (and for Lu_6MoSb_2) remain bonding to well above E_F. The lowest lying Lu−Te states correspond to particularly strong interactions with Lu1, the only close neighbor to Te, around −11 eV, and the weaker (longer) Te−Lu2 bonding. Again, the surface Lu1 atoms (with Te neighbors) tend to have positive charge, whereas all the inner atoms have stronger Lu−Lu bonding and relatively negative charges.[6] Naturally, Te has a negative charge. The innermost atom Lu3, which is not a Te neighbor, has the most negative charge, −0.32, and, in parallel, all of the strongest Lu−Lu bonding interactions.

(31) Herle, P. S.; Corbett, J. D. *Inorg. Chem.* **2001**, *40*, 1858.

Table 7. Selected Metal−Metal Distances (Å) and Mulliken Overlap Populations (MOP)

atom 1−atom 2	Sc_6OsTe_2	MOP	Lu_8Te	MOP
R1−R1, basal	3.152(4)	0.163	4.318(2)	0.032
R1−R1 along *c*	3.864(1)	0.109	3.687(2)	0.159
R2−R2, basal	4.114(3)	0.000	4.835(3)	0.045
R2−R2, along *c*	3.864(1)	−0.003	3.687(2)	0.272
R1−R2 (av)	3.30	0.095	3.59	0.240
i−o small TTP	3.223(2)	0.125	3.611(2)	0.210
o−i large TTP	3.448(3)	0.033	3.545(2)	0.300
R1−T′(R3)			3.283(2)	0.380
R2−T′(R3)			3.345(1)	0.353
T′−T′(R3BR3) (along *c*)			3.687(2)	0.242

Some selected metal−metal distances and MOP data for the two representatives Sc_6OsTe_2 (VEC = 38) and Lu_6TeLu_2 (VEC = 30) are listed in Table 7 for comparison. As before, the metal bonding in Sc_6OsTe_2 is expected to be more one-dimensional character in the TTP chain. The strongest bonding lies in the small TTP chain containing Os, namely, within the trigonal base, the i−o capping interactions and the R1−R1 interactions along *c* in decreasing magnitude. The large trigonal prism has nearly no metal−metal bonding. In contrast, the spread of bonding into a 3D metal network character in Lu_8Te is obvious. The strongest Lu−Lu bonding is within the larger Lu3-centered TTP; the weakest is in the small TTP around Te with a MOP only ∼8% of the largest one (0.032 vs 0.380). (Of course, the Coulomb contributions are doubtlessly in inverted order.) As a simple scale of 3D bonding character, the inter-TTP-chain interactions in these two examples have distinguishable differences; that in Lu_8Te (Lu2−Lu1, 3.61 Å, MOP 0.210) has a MOP value around 55% of that for the largest Lu−Lu interaction, whereas that in Sc_6OsTe_2 (Sc1−Sc2, 3.45 Å, MOP 0.033) is just ∼20% of the largest. The reason is more likely to be that Te at 2c sites is more electronegative and at lower energy, which drains more electron density from the Sc−Sc metal network than Lu3 does from the Lu−Lu network. The more polar Sc−Te interactions help the localization of the Sc−Sc interactions.

Conclusions

Both the crystal and electronic structures show that the 4d and 5d derivatives of Sc_6FeTe_2, namely Sc_6TTe_2 (T = Ru, Os, Ru, Ir), keep a dominant 1D TTP-chain character in the metal−metal bonding, but the Sc−T heteroatomic interactions become less polar with the heavier d period elements. The novel anti-typic $Sc_6Te_{0.8}Bi_{1.6}$ shows a nice size-determined site preference, as does Lu_8Te. The latter is also the first example in which the principal metallic element also occupies the interstitial site that is usually favored for a non-metal, and its metal−metal bonding tends to become more 3D with a lower VEC and fewer polar metal−non-metal interactions. The heavier variants of Fe_2P family, the electron-poorer Lu_8Te and Lu_6MoSb_2, show strong Lu−Lu interactions which give rise to broader Lu−Lu bonding bands. The diversity among Fe_2P structure type members in

terms of stoichiometries, electron counts, and bonding characteristics as well as in the chemical resemblance of neighboring elements, even metals and non-metals therein, illustrates some of the fascinating character of solid-state chemistry.

These results beg for some predictive output, i.e., regarding the stabilities of Lu_8Sb, Sc_6SbTe_2, Sc_6TSb, and the like. Unfortunately, the answers always depend on the relative stabilities of *alternate* products as well, many of which may involve now unknown compositions and structures. The synthetic experiment often gives the answer much more quickly and reliably.

Acknowledgment. We thank Marina Vondrova for assistance with the Sc_6TTe_2 reactions. This research was supported by the National Science Foundation, Solid State Chemistry, via Grants DMR-9809850 and -0129785 and was carried out in the facilities of the Ames Laboratory, U.S. Department of Energy.

Supporting Information Available: Tables of X-ray data collection and refinement results, anisotropic displacement parameters, and parameters used in extended Hückel calculations. This material is available free of charge via the Internet at http://pubs.acs.org.

IC0302581